AGU PUBLICATIONS

JGR

Journal of Geophysical Research: Space Physics

RESEARCH ARTICLE

10.1002/2016JA022972

Key Points:
- The IES observed cometary electron environment is well characterized with 2 kappa distributions
- The hot electron population is likely the solar wind halo electrons
- The warm electron population is a poorly understood minority, possibly of cometary origin

Correspondence to:
T. W. Broiles,
tbroiles@swri.edu

Citation:
Broiles, T. W., et al. (2016), Characterizing cometary electrons with kappa distributions, *J. Geophys. Res. Space Physics*, *121*, 7407–7422, doi:10.1002/2016JA022972.

Received 18 MAY 2016
Accepted 21 JUL 2016
Accepted article online 26 JUL 2016
Published online 12 AUG 2016
Corrected 23 AUG 2016

This article was corrected on 23 AUG 2016. See the end of the full text for details.

Characterizing cometary electrons with kappa distributions

T. W. Broiles[1], G. Livadiotis[1], J. L. Burch[1], K. Chae[1], G. Clark[2], T. E. Cravens[3], R. Davidson[4], A. Eriksson[5], R. A. Frahm[1], S. A. Fuselier[1,6], J. Goldstein[1,6], R. Goldstein[1], P. Henri[7], H. Madanian[3], K. Mandt[1,6], P. Mokashi[1], C. Pollock[8], A. Rahmati[9], M. Samara[10], and S. J. Schwartz[11,12]

[1]Space Science and Engineering Division, The Southwest Research Institute, San Antonio, Texas, USA, [2]The Johns Hopkins University Applied Physics Laboratory, Laurel, Maryland, USA, [3]Department of Physics and Astronomy, University of Kansas, Lawrence, Kansas, USA, [4]Department of Aerospace Engineering, University of Maryland, College Park, Maryland, USA, [5]The Swedish Institute of Space Physics, Kiruna, Sweden, [6]Department of Physics and Astronomy, University of Texas, San Antonio, Texas, USA, [7]Centre National de la Recherche Scientifique, LPC2E, CNRS, Orléans, France, [8]Denali Scientific, Healy, AK, USA, [9]Space Sciences Laboratory, University of California, Berkeley, California, USA, [10]NASA-Goddard Space Flight Center, Greenbelt, Maryland, USA, [11]Blackett Laboratory, Imperial College London, London, UK, [12]Laboratory for Atmospheric and Space Physics, University of Colorado Boulder, Boulder, Colorado, USA

Abstract The Rosetta spacecraft has escorted comet 67P/Churyumov-Gerasimenko since 6 August 2014 and has offered an unprecedented opportunity to study plasma physics in the coma. We have used this opportunity to make the first characterization of cometary electrons with kappa distributions. Two three-dimensional kappa functions were fit to the observations, which we interpret as two populations of dense and warm (density = 10 cm^{-3}, temperature = 2×10^5 K, invariant kappa index = 10−>1000), and rarefied and hot (density = 0.005 cm^{-3}, temperature = 5×10^5 K, invariant kappa index = 1–10) electrons. We fit the observations on 30 October 2014 when Rosetta was 20 km from 67P, and 3 AU from the Sun. We repeated the analysis on 15 August 2015 when Rosetta was 300 km from the comet and 1.3 AU from the Sun. Comparing the measurements on both days gives the first comparison of the cometary electron environment between a nearly inactive comet far from the Sun and an active comet near perihelion. We find that the warm population density increased by a factor of 3, while the temperature cooled by a factor of 2, and the invariant kappa index was unaffected. We find that the hot population density increased by a factor of 10, while the temperature and invariant kappa index were unchanged. We conclude that the hot population is likely the solar wind halo electrons in the coma. The warm population is likely of cometary origin, but its mechanism for production is not known.

1. Introduction

As comets approach the Sun, neutral gas escaping the nucleus becomes ionized, which creates an interesting plasma environment directly exposed to the flow of the supersonic solar wind. In situ observations of this dynamic plasma environment have been limited to a few brief flybys until very recently. Since 6 August 2014, the Rosetta spacecraft has escorted the comet 67P/Churyumov-Gerasimenko (67P), making ongoing observations of the plasma environment. Rosetta has already returned many interesting results, including deflection and mass loading of the solar wind, the acceleration of cometary pickup ions, electron heating, and the first observations of negatively charged solar wind hydrogen [*Nilsson et al*., 2015; *Goldstein et al*., 2015; *Burch et al*., 2015; *Broiles et al*., 2015; *Clark et al*., 2015; *Behar et al*., 2016]. Understanding the behavior of cometary electrons is particularly important, because they further ionize the coma and dust through electron impact ionization and play a role in plasma dynamics and chemistry [*Cravens et al*., 1987; *Cravens*, 1991; *Vigren and Galand*, 2013; *Mendis and Horányi*, 2013; *Rubin et al*., 2014].

Several previous missions have made observations of cometary electrons. The International Cometary Explorer (ICE) made a flyby through the tail of the comet Giacobini-Zinner (G-Z) on 11 September 1985. Additionally, cometary electrons were observed with the Giotto spacecraft, which did flybys of 1P/Halley (1P) on 14 March 1986 and then Grigg-Skjellerup (G-S) on 10 July 1992. The comet G-S had the lowest neutral production rate ($Q \approx 6.7 \times 10^{27}\ s^{-1}$), while G-Z had an intermediate neutral production rate ($Q \approx 2.0 \times 10^{28}\ s^{-1}$), and 1P had the highest production rate ($Q \approx 6.9 \times 10^{29}\ s^{-1}$).

Bame et al. [1986] performed a moment analysis of the electron data from the ICE spacecraft, which made a flyby of G-Z with a closest approach of 7800 km in the comet's plasma tail. Based on the density, speed, and

temperature of the electrons, *Bame et al*. concluded that ICE had traveled through six distinct regions. From farthest to closest to the comet, the regions were described as pristine solar wind ($7\,cm^{-3}$; $500\,km\,s^{-1}$; 2×10^5 K), transition region ($10\,cm^{-3}$; $400\,km\,s^{-1}$; 4×10^5 K), sheath ($10\,cm^{-3}$; $200\,km\,s^{-1}$; 3×10^5 K), boundary layer ($50\,cm^{-3}$; $50\,km\,s^{-1}$; 1.5×10^5 K), cold intermediate coma ($100\,cm^{-3}$; $0\,km\,s^{-1}$; 7×10^4 K), and plasma tail ($200\,cm^{-3}$; $0\,km\,s^{-1}$; 7×10^4 K). *Bame et al*. also noted periodic density and temperature variations in the transition region and sheath that were anticorrelated. This excluded the possibility of an upstream, fast-mode shock, but opened the possibility of heating through pickup ion-driven instabilities.

In a similar study, *Zwickl et al*. [1986] fit the same data set with three Maxwellian distributions to provide density and temperature measurements for each population. They found that the cometary electrons were well described by three populations, which they characterize as cold ($200\,cm^{-3}$; 3×10^4 K), mid ($20\,cm^{-3}$; 1×10^5 K), and hot ($0.1\,cm^{-3}$; 8×10^5 K). Additionally, *Zwickl et al*. [1986] found that density and temperature shared an inverse relationship for the cold and hot population. In the low-energy and high-energy populations, the lowest temperatures and highest densities were observed near the closest approach to the comet. In contrast, the midpopulation had higher densities near the comet's flanks, but there was also a local maximum near closest approach. They concluded that the cold and midpopulation were likely of cometary origin [*Ashihara*, 1978; *Cravens*, 1987; *Gan and Cravens*, 1990; *Marconi and Mendis*, 1986; *Häberli et al*., 1996], and the hot population was likely the solar wind halo electrons [*McComas et al*., 1992].

Thomsen et al. [1986] found that cometary electrons could be described with a flattop distribution, and that this behavior was similar to electrons observed elsewhere in the heliosphere that had passed through a weak shock [*Feldman et al*., 1983; *Feldman*, 1985; *Scudder*, 1995]. *Thomsen et al*. concluded that this was evidence of wave heating caused by a bow shock ahead of G-Z, which became intermittent along the flanks. *Clark et al*. [2015] used a similar approach to perform the first study of cometary electron evolution around 67P. At 67P the increased count rate below 100 eV was observed well beyond 3 AU from the Sun, where a shock was not expected or observed [*Clark et al*., 2015]. Consequently, *Clark et al*. suggested that cometary electron heating was likely due to an admixture of photoelectrons and waves produced by the pickup ion instability.

The flattop distribution was a useful diagnostic tool for characterizing distributions that were not in thermal equilibrium. However, the flattop distribution lacks the physical meaning of a distribution developed with the mathematical formalism of statistical mechanics. There have been many recent advances for systems and specifically plasmas out of thermal equilibrium [*Tsallis*, 1988; *Livadiotis and McComas*, 2009, 2011, 2013a, 2013b; *Livadiotis*, 2015, and references therein]. This work has resulted in a new form of the kappa distribution originally described by *Vasyliunas* [1968]. Kappa distributions are useful in the characterization of solar wind electrons, particularly the halo and strahl electrons [*Maksimovic et al*., 2005; *Štverák et al*., 2009]. However, much of the work surrounding kappa distributions was developed relatively recently, and its application to cometary electrons has never been considered.

In this paper we characterize the suprathermal electrons surrounding the comet 67P/Churyumov-Gerasimenko using Tsallis statistical mechanics. Additionally, we developed a novel technique to calibrate electron spectrometers using flight data. We used calibrated observations from the ion and electron sensor (IES) on 30 October 2014 and 15 August 2015 when the comet was far from the Sun and near perihelion, respectively. Each measurement is fit with the summation of 2 kappa distributions with isotropic temperatures. We find that the measurements on both days are generally well fit by this approach and in agreement with the work of *Bame et al*. [1986] and *Zwickl et al*. [1986]. We then compared the results between 3 AU and 1.3 AU to understand how the different electron populations evolve as the comet approaches the Sun.

2. Instrumentation

2.1. The Ion and Electron Sensor (IES)

The ion and electron sensor (IES) includes the only electron spectrometer on board Rosetta. IES measures energies per charge between 4.3 eV/q and 18 keV/q, with a $\Delta E/E$ of 8%, and has a $360°\times90°$ field of view with an angular resolution of $22.5°\times6°$ for electrons [*Burch et al*., 2007]. Measurements are made at a variable cadence, between 128 and 1024 s. However, it is impossible to simultaneously return all of the above-mentioned energy, angular, and time resolution within telemetry constraints. Consequently, measurement modes are used to reduce the complexity of the data in order to meet specific science goals within data volume limits.

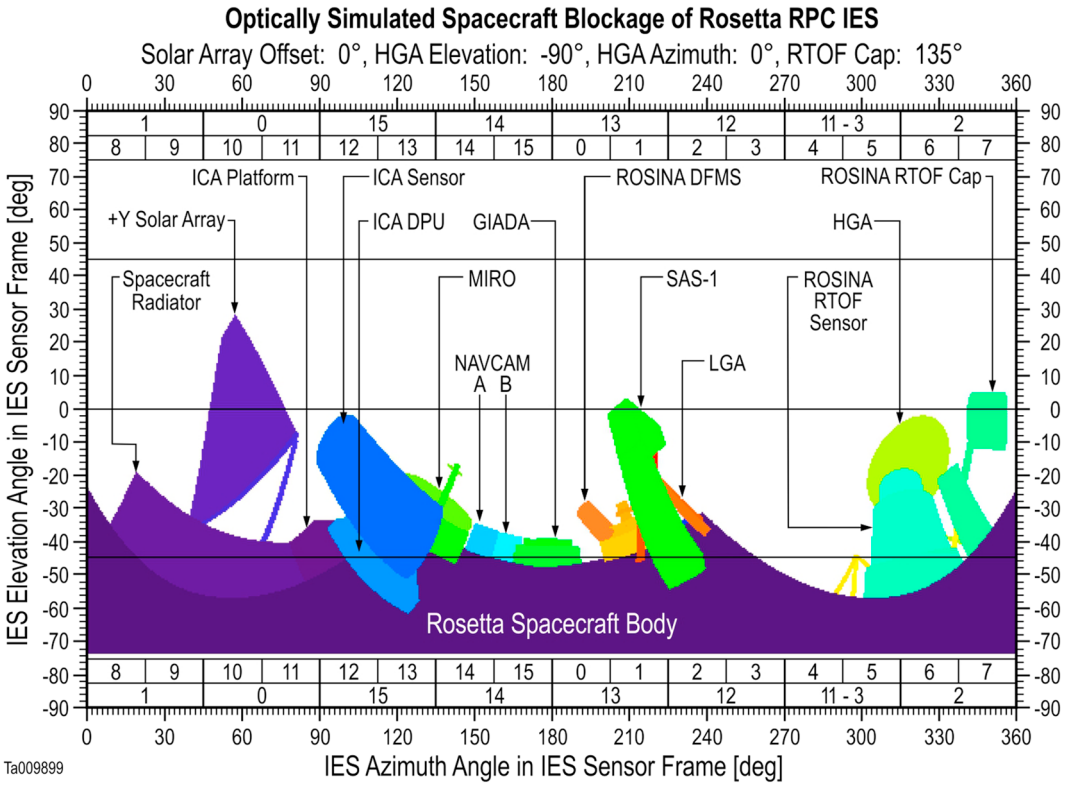

Figure 1. A simulation showing known objects with IES' field of view [*Acton*, 1996]. The azimuthal ranges of IES' ion and electron anodes are marked above and below the figure, respectively, as the outer and inner labels.

2.2. Flight Calibration of the Electron Sensor

We have developed a technique to calibrate the electron sensor using all of the flight data from 1 January 2015. The ion and electron sensor was calibrated in the laboratory before launch. However, laboratory calibration is unable to account for factors like spacecraft blockages, differential sensitivity between aging microchannel plates, or intangible effects such as aging of sensor components.

Our approach is to assume isotropy in the rest frame of the cometary electron distribution, and that at least one of IES' look directions has the optimal geometric factor described by *Burch et al.* [2007] (i.e., 5×10^{-9} m^2 sr eV/(eV counts/electron)). An isotropic electron distribution is a reasonable assumption based on results by *Zwickl et al.* [1986]. We consider the ideal look direction to be free of spacecraft blockages, generally sunward pointing, and near 0° elevation in IES' field of view. We consider low elevation directions to be more ideal, because the values calculated in Table 1 of *Burch et al.* [2007] are specified for 0° elevation (G. Miller, private communication, 2015).

Figure 1 characterizes the spacecraft blockages relevant to IES. Anode 3 is free of blockages and is generally pointed sunward. Consequently, we select anode 3 at elevation step 9 as the optimal look direction, which corresponds to azimuth range 247.5°–270° and elevation range 0° to +6° in the IES coordinate system. Comparing each look direction to an ideal case is most effective when IES is using a measurement mode that has high spatial resolution, and for this reason we have limited calibration to high telemetry rate modes with 1024 s time resolution. Moreover, this technique needs a statistically significant number of counts, and results are improved by integrating multiple measurement cycles together.

We compare the observed counts at every look direction to that of our ideal direction at each energy step. Equation (1) describes our method for calculating the calibrated geometric factor, G′, using observed counts summed over time, *C*, at each azimuth step, *i*, elevation step, *j*, energy step, *k*, and the published geometric factor, *G* [*Burch et al.*, 2007].

$$G'_{i,j,k} = \frac{C_{i,j,k}}{C_{3,\,9,\,k}} G \tag{1}$$

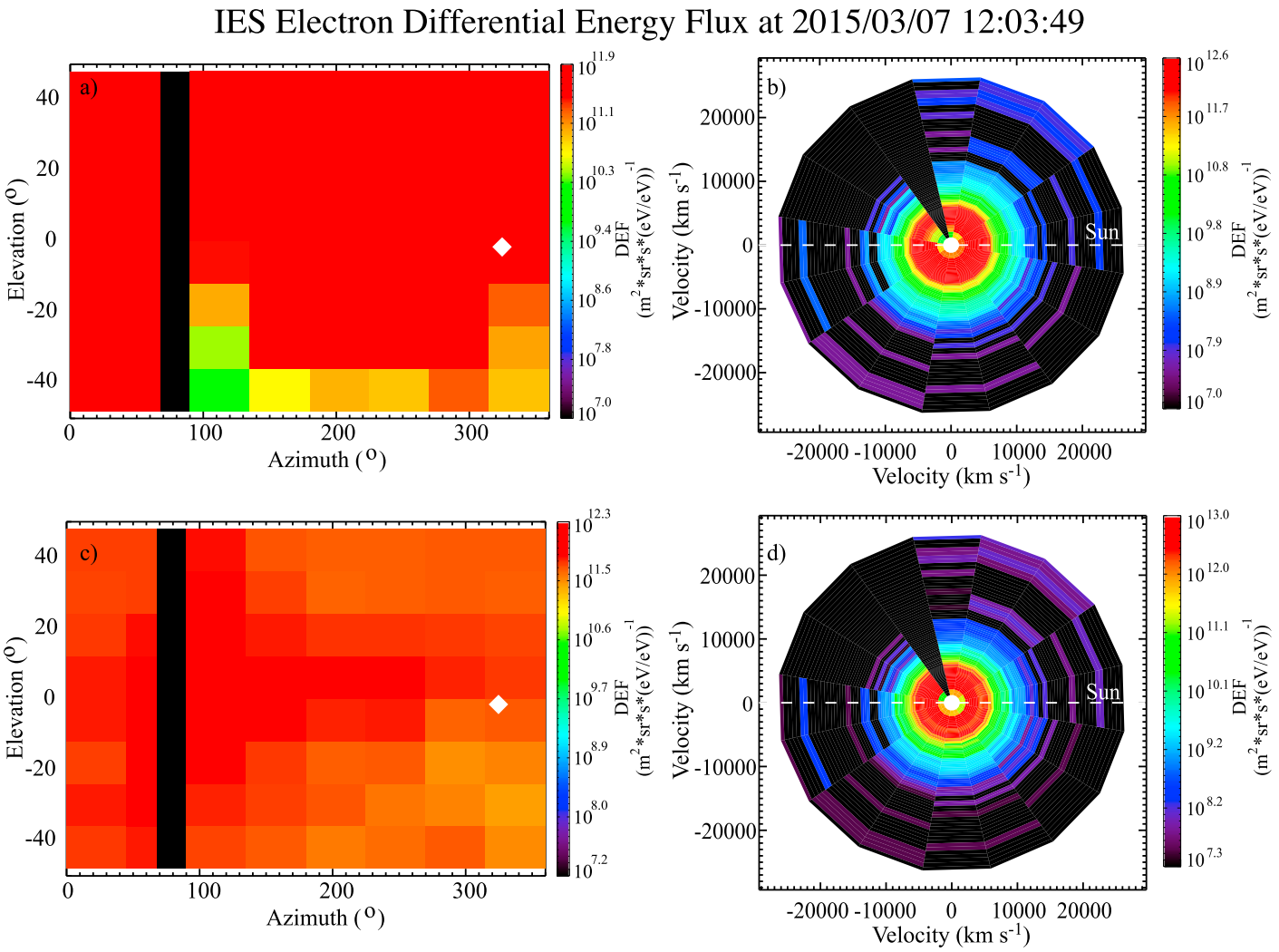

Figure 2. A comparison of IES DEF, for a single measurement on 7 March 2015 at 12:03:09, using a (a and b) constant geometric factor and a (c and d) flight-calibrated geometric factor. Figures 2a and 2c show DEF in elevation and azimuth space, averaged over all energies. The white diamond in Figure 2 shows the position of the Sun in IES' field of view. Figures 2b and 2d show electron DEF in velocity space averaged over all elevations. The white dashed line shows the spacecraft Sun line. The black strip between azimuths 67.5° and 90° in Figures 2a and 2c, and black wedge in Figures 2b and 2d are caused by missing data that are no longer returned due to a noisy anode.

Equations (2) and (3) describe our estimate of the uncertainty of G′ using error propagation of equation (1). Uncertainty in $C_{i,j,k}$ is estimated with Poisson statistics, and G is treated as a known constant. Covariance between counts at azimuth i and elevation j, and azimuth 3 and elevation 9, $\sigma_{ij,39,k}$, is estimated using the series of data that is integrated to calculate $C_{i,j,k}$.

$$\Delta G'^{2}_{i,j,k} = \sigma^{2}_{i,j,k}\left(\frac{\partial G'_{i,j,k}}{\partial C_{i,j,k}}\right)^{2} + \sigma^{2}_{3,9,k}\left(\frac{\partial G'_{i,j,k}}{\partial C_{3,9,k}}\right)^{2} + 2\sigma_{ij,39,k}\left(\frac{\partial^{2} G'_{i,j,k}}{\partial C_{i,j,k}\partial C_{3,9,k}}\right) \tag{2}$$

$$\Delta G'^{2}_{i,j,k} = \left(\frac{C_{i,j,k}}{C^{2}_{3,9,k}} + \frac{C^{2}_{i,j,k}}{C^{3}_{3,9,k}} - \frac{2\sigma_{ij,39,k}}{C^{2}_{3,9,k}}\right)G^{2} \tag{3}$$

Figure 2 shows a comparison of IES flux observations from 7 March 2015 with the application of a constant geometric factor (Figures 2a and 2b) and the new, flight-calibrated geometric factor developed from measurements taken on 1 January 2015 (Figures 2c and 2d). Figures 2a and 2c contain spectrograms of electron flux averaged over energy with azimuths along the abscissa and elevations along the ordinate. Figures 2b and 2d show spectrograms of electron differential energy flux (DEF) averaged over all elevations, in a polar

coordinate system where energy and azimuth correspond to the radial position and the azimuthal position, respectively. The color bar is scaled from the estimated background level of the instrument to the peak DEF of each figure to show absolute variations rather than relative variations between pixels. Variations in the average differential energy flux across anodes and elevations are indicated by changes in the colors represented in Figures 2a and 2c. The spectrograms using the flight-calibrated geometric factor have more isotropic DEF as indicated by a nearly flat average differential energy flux in Figure 2c and the circularity in Figure 2d. We note that data are no longer returned from anode 11 (azimuths 67.5°–90°) due to noise, which causes these azimuths to be completely black in the spectrograms.

In April 2015, the electron sensor's response began to change. Anodes 8–15 in the electron sensor started measuring reduced DEF at lower energies in spite of the new flight calibration. Initially, it was thought to be a physical effect related to cometary evolution. However, the DEF anisotropy was later found invariant of spacecraft rotation or position, which strongly suggests that it is an instrumental effect.

The most likely cause for the reduced sensitivity in half of the electron sensor's anodes is a threshold change in one of its octal amplifiers. The electron sensor has two charge-sensitive octal amplifiers, which each enhances the signals of eight anodes. Amplifier 1 is responsible for anodes 0–7, and amplifier 2 is responsible for anodes 8–15. Each amplifier has one threshold setting for its group of anodes configured during fabrication. The anodes of amplifier 2 correspond exactly with our loss in differential energy flux. The behavior of amplifier 2 is not well understood, but the threshold setting is highly suspect since a change in the threshold level will affect the amplification of all anodes within its group. Amplifier power and ground are also common to all anodes within the amplifier's group, but they are also common to both amplifiers: efforts at understanding the cause are ongoing. Nevertheless, we are confident that we can still use the measurements after April 2015 in our study, as we will show below.

3. Results

3.1. Observations

Figure 3 shows the evolution of the cometary electron environment in the year leading up to perihelion. Each month is separated into individual panels. As shown by *Clark et al*. [2015], the count rates below 100 eV steadily increased until December 2014. However, the count rate peaked in January or February of 2015 and then gradually decreased with time. To understand why the intensity of low-energy electrons has decreased near perihelion (13 August 2015), we have performed case studies on 2 days of observations that are representative of the inactive and active comet. We have marked the approximate time of both days in Figure 3 as vertical, black dashed lines along with a red arrow and label. The first day is 30 October 2014 when the comet was ~3.1 AU from the Sun and ~30 km from Rosetta. The second day of data was measured on 15 August 2015 when the comet was ~1.3 AU from the Sun and ~350 km from Rosetta. We note that black regions occur where no data was collected.

Figure 4 shows electron DEF over the entire day of 30 October 2014. Figure 4a shows the average DEF at each E/q step versus time, Figure 4b shows the average DEF at each elevation step versus time, and Figure 4c shows the average DEF at each azimuth versus time. The solid and dashed lines in Figures 4b and 4c, respectively, show the position of the Sun and 67P in IES' field of view. The vertical, dashed lines mark the times of case studies that will be discussed in Figure 6. The black pixels in Figure 4c are unreturned data due to a noisy anode. These observations were made when 67P was outside of the heliocentric distance where water is significantly sublimated and are representative of the electron environment around a nearly inactive comet. Similar to Figure 2, the color bar is intentionally scaled from the background threshold of the instrument to the peak DEF in order to show absolute variations.

The electron DEF remains largely isotropic (Figures 4b and 4c) over the entire day of 30 October 2014. However, the mid-energy DEF (Figure 4a) varies significantly over the course of the day. The plasma environment around 67P is highly dynamic with the shortest interval variations occurring on timescales shorter than IES' measurement cycle, as observed from the Rosetta Langmuir Probe (LAP) instrument and the Mutual Impedance Probe (MIP) [*Eriksson et al*., 2006; *Trotignon et al*., 2006]. However, variations also occur on longer timescales; an intermediate duration event occurs between 06:00 and 07:00, and a longer duration interval is observed between 11:00 and 18:00.

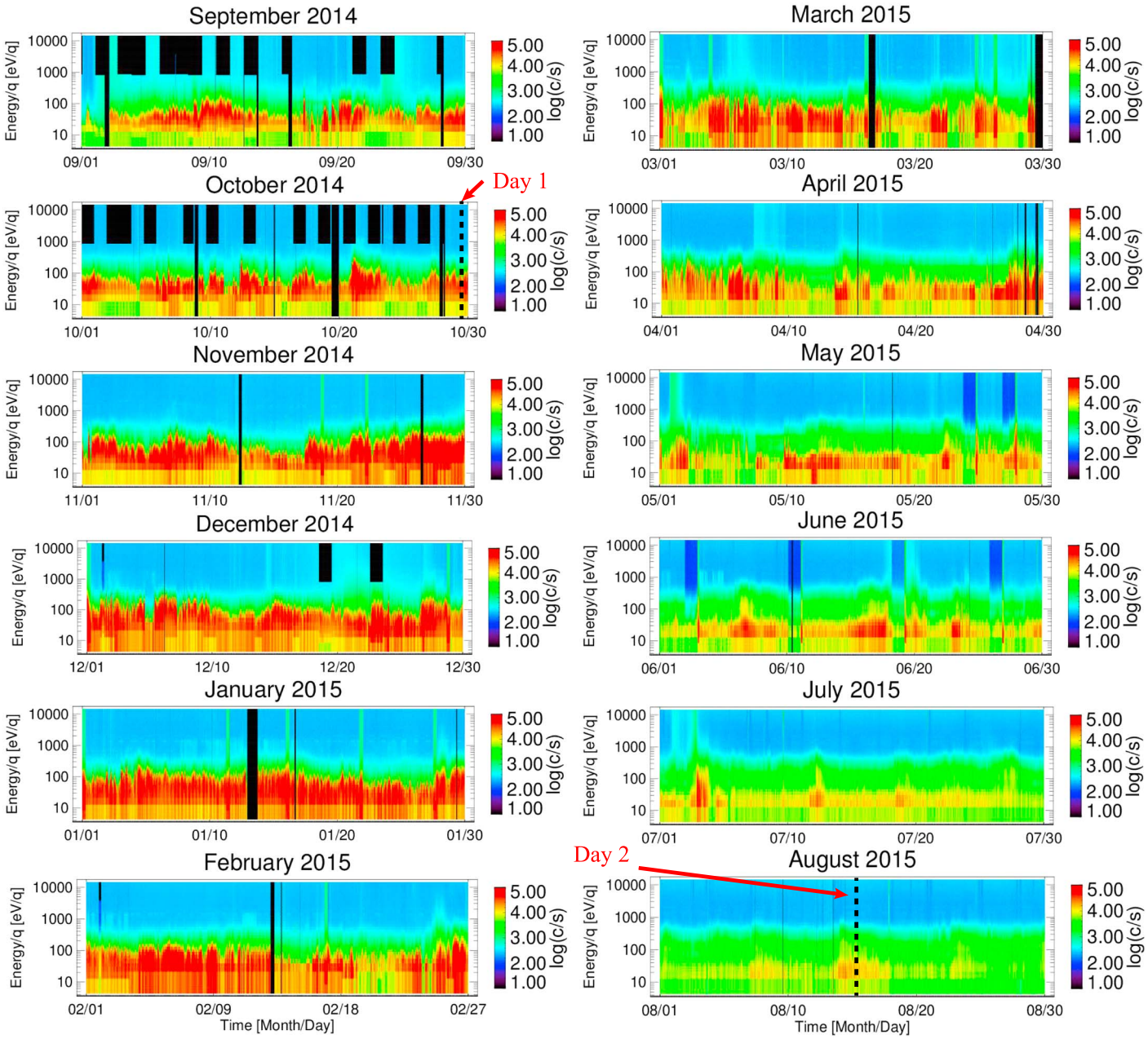

Figure 3. The IES electron count rate for each energy over time from 1 September 2014 to 1 September 2015. Each month is shown in an individual panel. The observations of an inactive and active coma were, respectively, made on 30 October 2014 (Day 1) and 15 August 2015 (Day 2) and marked by vertical, black, dashed lines.

Figure 5 shows IES electron DEF over the entire day of 15 August 2015 in the same format as in Figure 4. These observations were made near perihelion and are representative of IES electron measurements made during 67P's high activity but farther from the comet. The variability in the mid-energy flux is still present, but the high rates of DEF have receded to lower energies (Figure 5a). We also note the contrast in DEF between azimuths greater than and less than 180° (Figure 5c), which is an instrumental effect discussed in section 2.2.

3.2. Fitting Technique

The DEF shown in Figures 4 and 5 can be converted to a velocity space density and fit with statistical models that characterize the parameters of the electrons such as density and temperature. Equations (4)–(7) below define the model used to characterize the IES electron data.

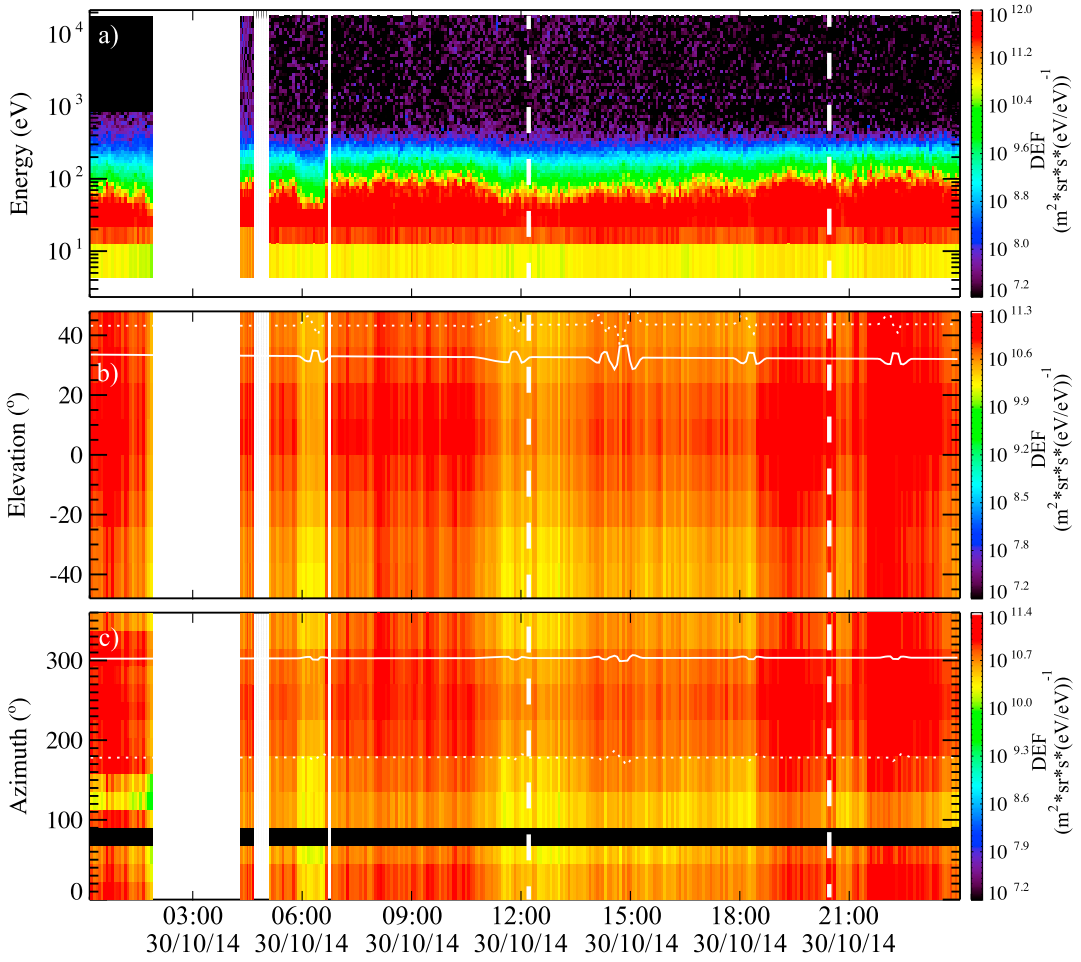

Figure 4. Average DEF for (a) *E/q* versus time, (b) elevations versus time, (c) and azimuths versus time for 30 October 2014. Vertical dashed lines mark times case studies discussed in Figure 5. Horizontal solid and dotted lines in Figures 4b and 4c, respectively, show the position of the Sun and 67P in IES' field of view.

$$f = f_W + f_H + f_{BG} \tag{4}$$

The model, f, is the sum of a warm distribution, f_W, a hot distribution, f_H, and a constant background converted to a phase space density, f_{BG}.

$$f_W = \frac{n_W}{\left(\kappa_{W0}\pi\left(\frac{2kT_W}{m_e}\right)\right)^{\frac{3}{2}}}\frac{\Gamma\left(\kappa_{W0}+\frac{5}{2}\right)}{\Gamma(\kappa_{W0}+1)}\left[1+\frac{(v_x-\langle v_x\rangle)^2+\left(v_y-\langle v_y\rangle\right)^2+(v_z-\langle v_z\rangle)^2+\frac{2q\varphi_{SC}}{m_e}}{\kappa_{W0}\left(\frac{2kT_W}{m_e}\right)}\right]^{-\kappa_{W0}-\frac{5}{2}} \tag{5}$$

The warm distribution (equation (5)) is a kappa function as defined in equation (3.5) of *Livadiotis and McComas* [2013a] and is characterized by the following seven parameters: density, n_W, bulk velocity vector, $<v_x>$, $<v_y>$, $<v_z>$, temperature, T_W, spacecraft potential, φ_{SC}, and an invariant kappa index, κ_{W0}. We will refer to the magnitude of the bulk velocity vector as v_w. The spacecraft potential is determined using data from LAP as described by *Odelstad et al.* [2015]. If LAP data is unavailable, φ_{SC} is assumed to be 0 V, which may affect the estimated bulk velocity and density. We note that the warm population is comparable in energy to the midpopulation discussed by *Zwickl et al.* [1986].

$$f_H = \frac{n_H}{\left(\kappa_{H0}\pi\left(\frac{2kT_H}{m_e}\right)\right)^{\frac{3}{2}}}\frac{\Gamma\left(\kappa_{H0}+\frac{5}{2}\right)}{\Gamma(\kappa_{H0}+1)}\left[1+\frac{v_x{}^2+v_y{}^2+v_z{}^2}{\kappa_{H0}\left(\frac{2kT_H}{m_e}\right)}\right]^{-\kappa_{H0}-\frac{5}{2}} \tag{6}$$

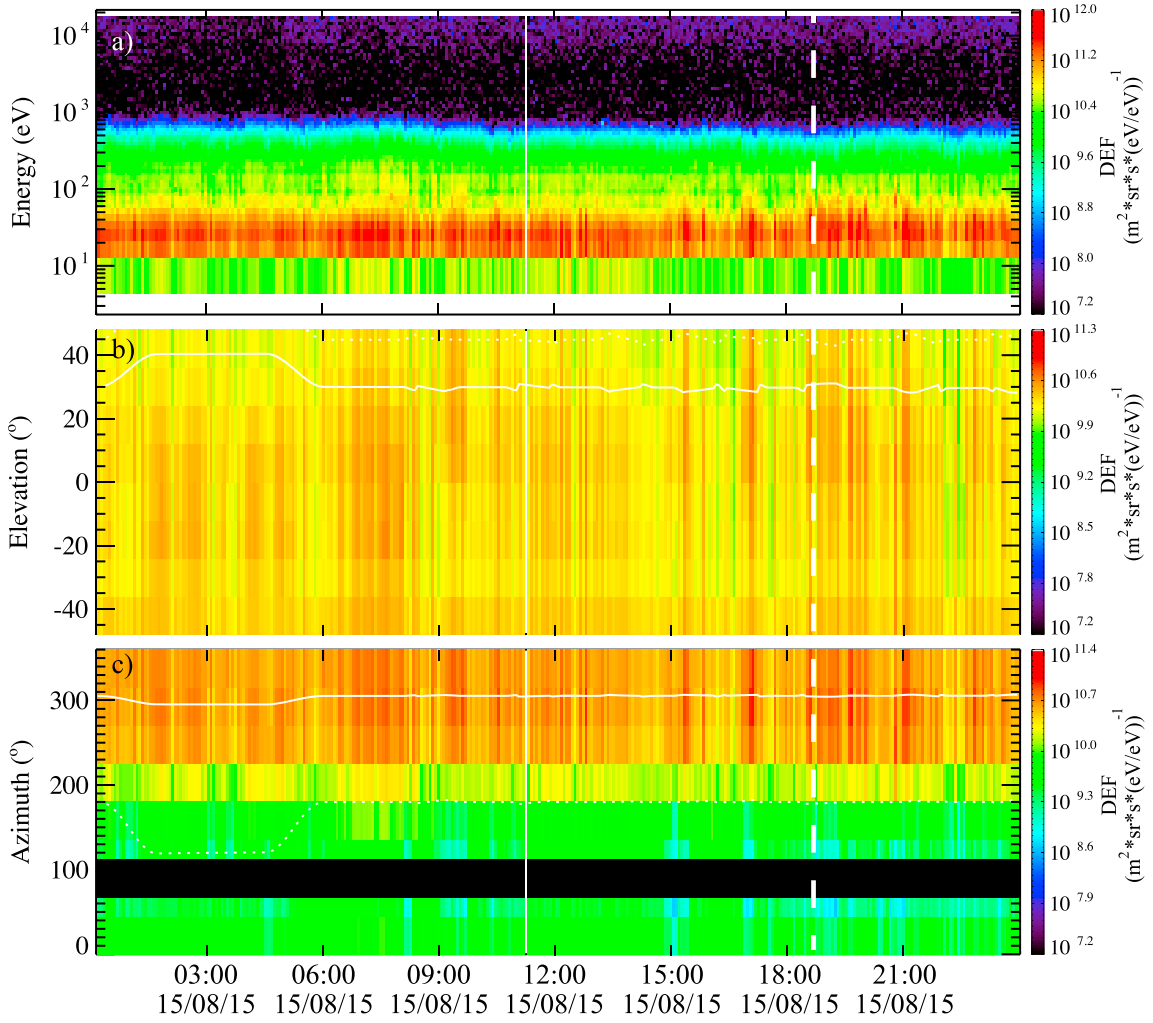

Figure 5. Average DEF from IES' electron sensor for 15 August 2015 in the format of Figure 4.

The hot distribution (equation (6)) is also a kappa function with the same mathematical form, but its bulk velocity vector and spacecraft potential are assumed to be negligibly small. The hot population is also the same as discussed by *Zwickl et al*. [1986].

The background noise level of the IES (equation (7)) is an assumed constant count rate of 1.2 counts/s, divided by the total geometric factor of the instrument defined by *Burch et al*. [2007], *G*, and particle speed, *v*, to the fourth power.

$$f_{BG} = \frac{2 \times 1.2}{v^4 G} \tag{7}$$

As discussed in sections 2.2 and 3.1, half of the data from the electron sensor became unreliable after April 2015. This change in instrument behavior is poorly understood and has evolved over time. Consequently, we only use the data from anodes 0–7 for our fitting analysis. We also use this approach for the measurements taken before April for consistency.

The spacecraft potential, bulk velocity of the hot distribution, and background count rate are all fixed values in our fitting analysis. However, the remaining nine parameters are varied with the Levenberg-Marquardt algorithm such that the χ^2 is minimized for each measurement. The computed moments of each measurement set the initial values for each fit.

Figure 6 shows three case studies of our fitting analysis for measurements annotated by the vertical dashed lines in Figures 4 and 5. Figures 6a–6c contain data from measurements at 30 October 2014 12:03:13, 30

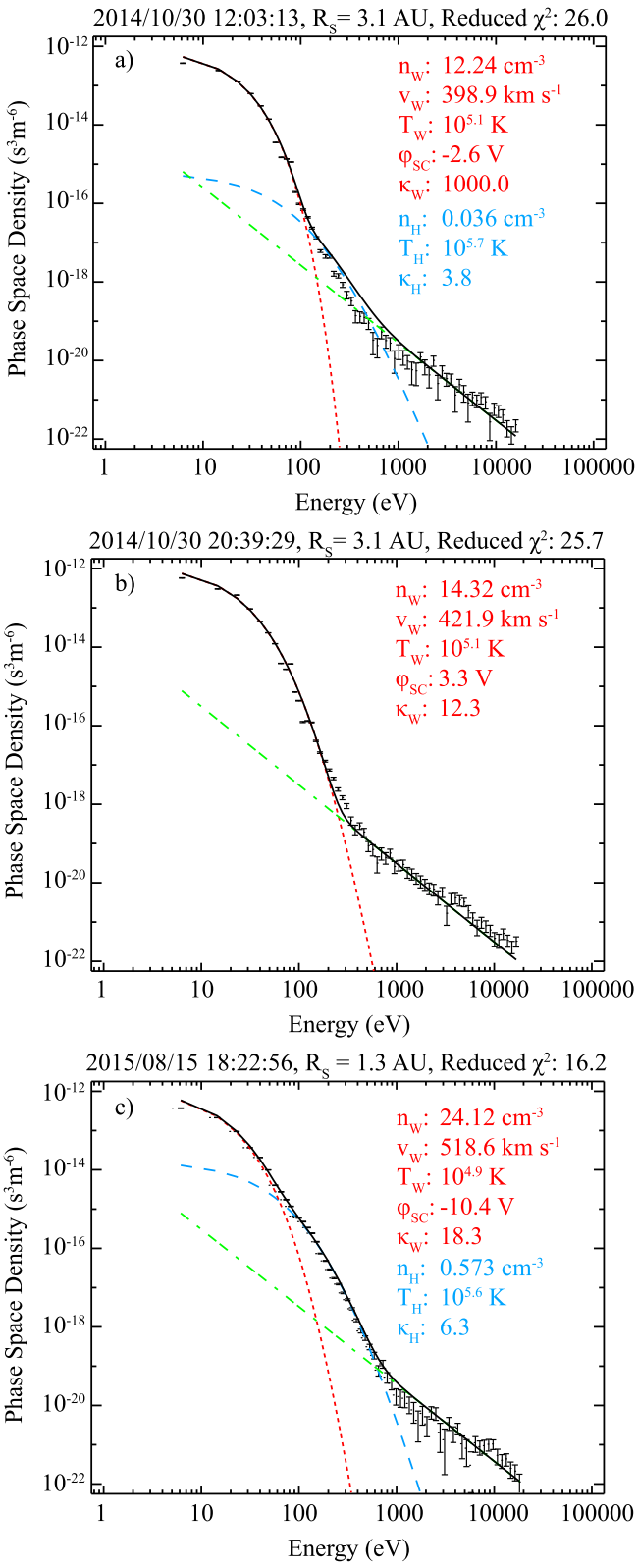

Figure 6. Case studies comparing fitting results to individual IES measurements. Vertical black bars, observed phase space density and uncertainty; dotted red curve, the kappa distribution fit to the warm electron population; dashed blue curve, the kappa distribution fit to the hot electron population; dash-dotted green line, constant instrument background; and solid black curve, the sum of the three previously mentioned distributions. Key parameters of the warm and hot distribution are, respectively, listed in the upper right corner of each panel as red and blue text.

October 2014 20:39:29, and 15 August 2015 18:22:56, respectively. Each fit was made with the velocity space in anodes 0–7 and is summed over these azimuths and all elevations for visualization. The observed phase space density and their uncertainty are represented by vertical black bars, while f_W, f_H, and f_{BG} are, respectively, shown as dotted red, dashed blue, and dash-dotted green curves. The total of all three functions is represented by the solid black curve.

There are several important results in Figure 6. Visual comparison of the observations to our model appears reasonable for all three measurements. However, the reduced χ^2 of each measurement is larger than 1, suggesting that our model underfits the observations (i.e., the model fails to capture the complete relationship between observed phase space density and velocity). Two likely explanations for the model underfitting the observations are as follows: (1) our model incorrectly assumes that the electrons all have an isotropic temperature, and (2) our attempts to correct for instrumental effects are imperfect. The density of the warm electron population is ~5.5–14.3 cm^{-3} in all three measurements. Similarly, the warm electron temperature is consistently near 10^5 K. The warm population's κ_0 is in the range of 12.3–26.3, which is too large to be considered out of thermal equilibrium ($\kappa_0 > 1$), but it still produces a spectral tail that is clearly not Maxwellian [*Livadiotis et al.*, 2013]. In the case of

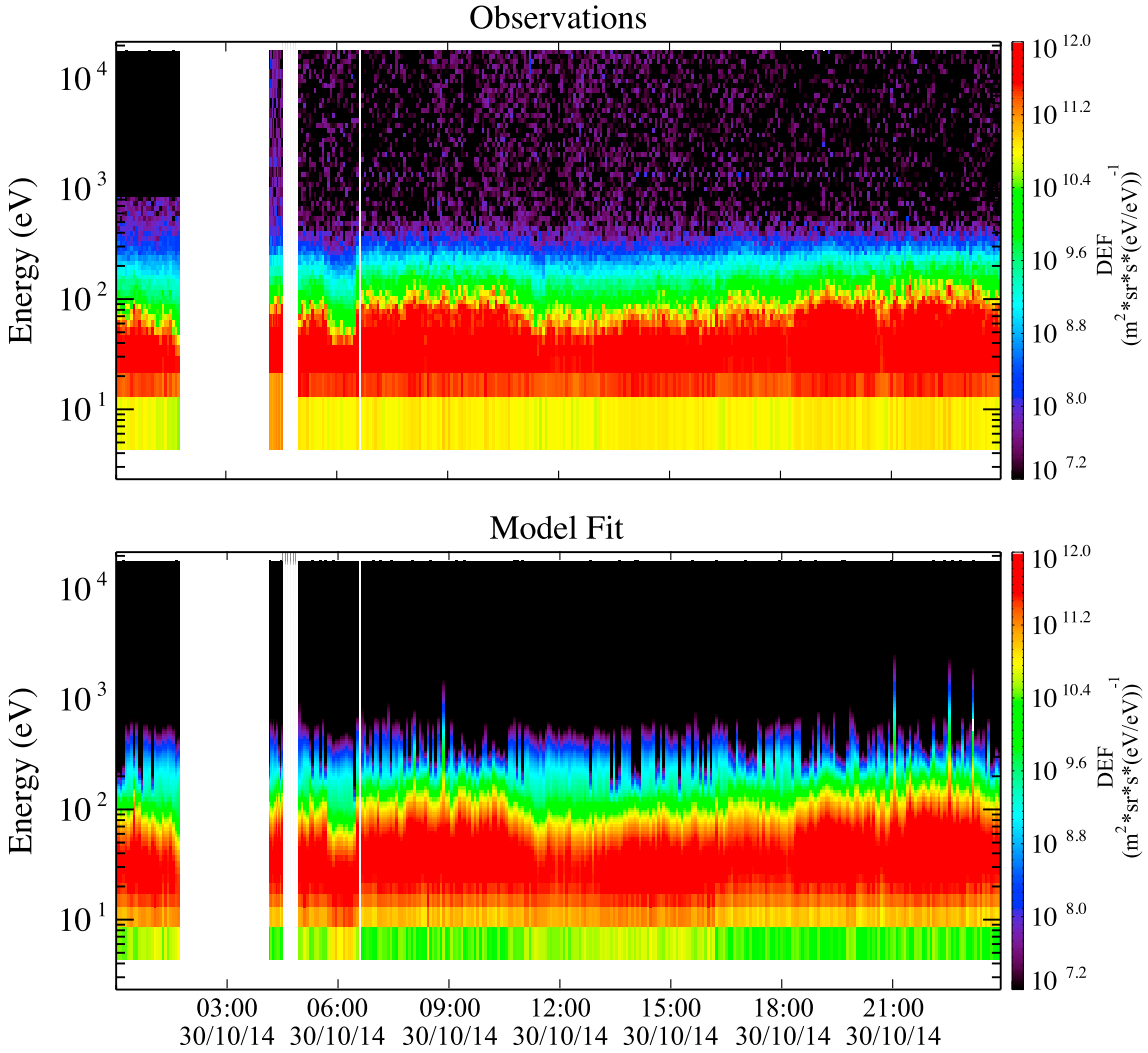

Figure 7. (top) A qualitative comparison of the observations on 30 October 2014 with the (bottom) sum of the fitted distributions of warm and hot electrons.

the measurement at 30 October, 20:39:29 (Figure 6b), we find that the warm electron population is so dense and has a sufficiently low κ_0 that the hot electron population is completely hidden. We find that the masking of the hot distribution occurs much more regularly in the measurements far from the Sun relative to those near perihelion.

We have also performed a qualitative comparison between observations from 30 October 2014 and our fitted model results. The results of this comparison are presented in Figure 7. Figure 7a shows the observed DEF at each energy step over time, while Figure 7b shows the same quantity computed from the fitted model described in equation (4). We note that the model does an excellent job of reproducing the energy spectrum of DEF throughout the day. In particular, we find that the model recreates the variability of DEF below 100 eV/q. Below 20 eV, the model tends to underestimate the DEF, which might be explained by a third, cold electron population that IES lacks the resolution to model. At higher energies, the model DEF is too large because the hot population is consistently overestimated by a factor of 2 or 3. The intermittent dropouts of higher-energy DEF occur when the modeled hot population is negligible relative to the warm population and background. In summary, the observed DEF is reasonably recreated by the two modeled kappa distributions.

3.3. Fitting Results

Figure 8 shows the results of our fitting analysis for the entire day of 30 October 2014. Figures 8a–8e include time series of density (a), bulk speed (b), temperature (c), κ_0 values, and a reduced χ^2 estimate of goodness of

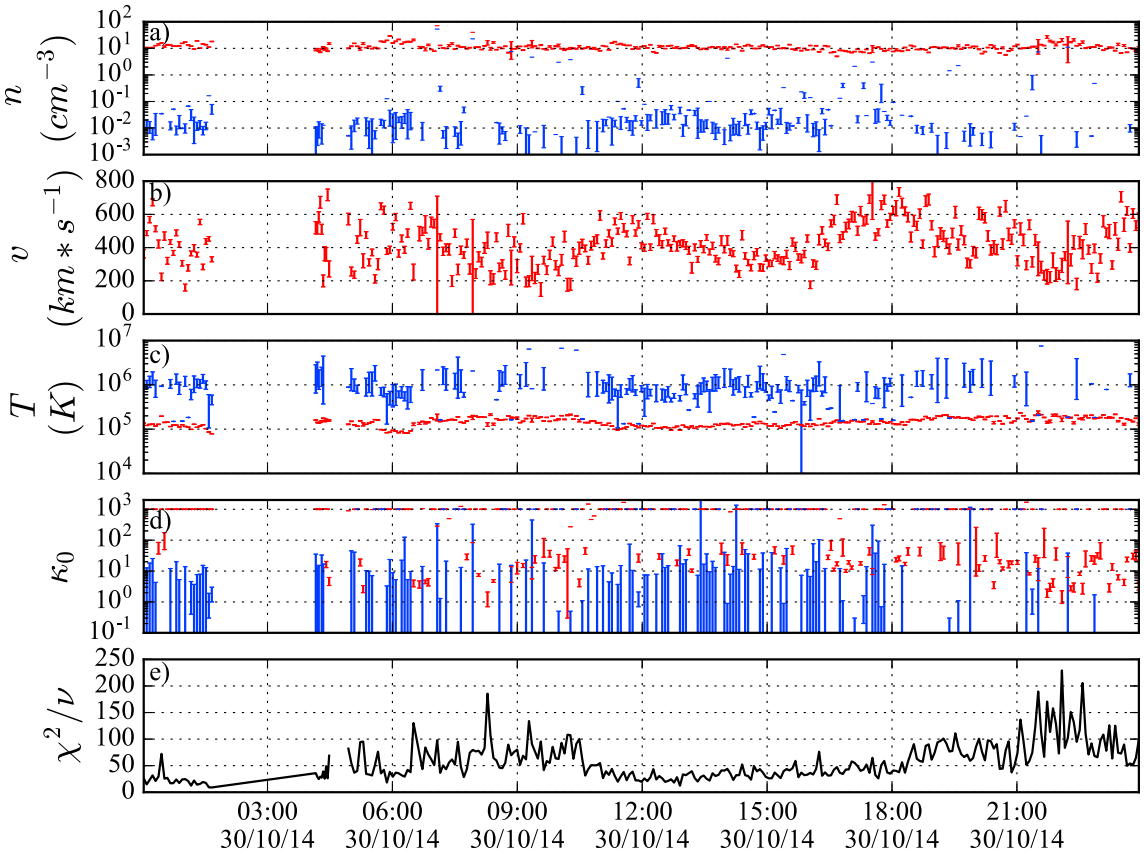

Figure 8. A time series of model fit results with uncertainty for 30 October 2014. (a) Electron density, (b) bulk velocity, (c) electron temperature, (d) κ_0 values, and (e) reduced χ^2. Fit parameters are colored red or blue to indicate whether they belong to the warm or hot population, respectively.

fit. Red data are used for parameters from the warm population model, and blue data are used for parameters from hot population model. We note that the reduced χ^2 is computed by dividing the χ^2 of the fit by the number of degrees of freedom, ν.

The warm population's density (Figure 8a, red data) on 30 October 2014 was fairly stable between 10 and 30 cm^{-3}. In contrast, the density of the hot population (Figure 8a, blue data) had more variation between 0.005 and 0.1 cm^{-3}, but this variation is comparable in size to the parameter uncertainty and may not be statistically significant. The bulk velocity of the warm population (Figure 8b) varied between 200 and 600 km s^{-1}. The interpretation of this fitted velocity as a real velocity of the electron distribution is highly uncertain. Anisotropies in the particle distribution or in the instrument sensitivity will give rise to nonzero bulk velocity values in the fit even if no such drift actually exists, particularly for an instrument with limited field of view. Expected values of such errors could be some significant fraction of the thermal speed. Comparing to the warm population thermal velocity of about 1000 km/s, our values are in that range. While the data do not exclude a significant electron drift, the fitted v_w values should not be taken as unambiguous evidence for drift speeds at solar wind range. The warm population temperature (Figure 8c, red data) varied between 1×10^5 and 3×10^5 K (8.6–25.9 eV) with an approximate 12 h periodicity between peaks (09:00 and 21:00). The comet's rotation also has a 12 h period, which suggests that variations in the warm population are related to local neutral variations [*Hässig et al.*, 2015]. The hot population's temperature (Figure 8c, blue data) is also variable, but the variation is comparable to the uncertainty in this parameter and we do not consider this to be statistically significant. The κ_0 of the warm population (Figure 8d, red data) is highly variable and ranges from 1 to 1000, ($\kappa_0 = 1000$ is the numerical approximation of infinity in the model, meaning that the electron distribution shape is Maxwellian). The κ_0 of the hot population (Figure 8d, blue data) range from 0.1 to 1000, but we believe the values of 1000 are the result of imperfect fitting and not physical. The reduced χ^2 of the fit ranges from 20 to 220, but most values are

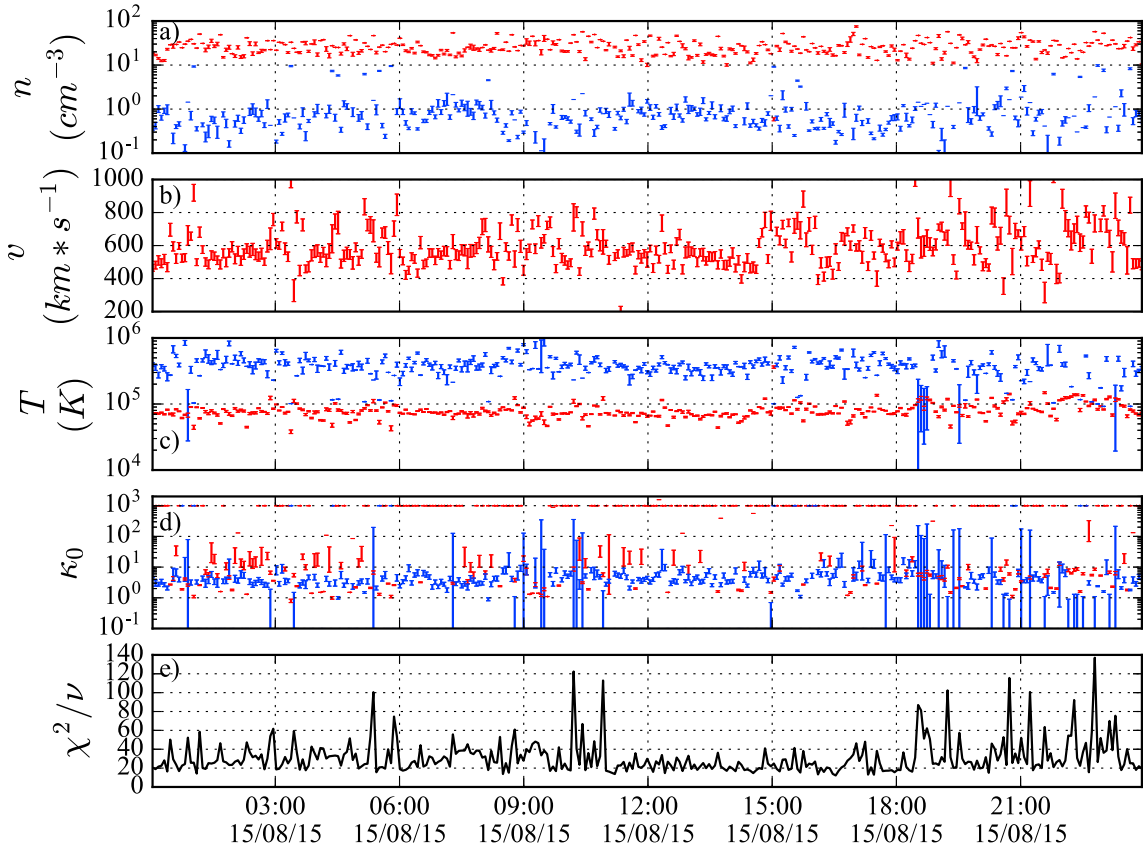

Figure 9. A time series of model fit results for 15 August 2015 in the same format as Figure 8.

less than 100. Additionally, we note that the reduced χ^2 also has a 12 h periodicity and appears correlated with the warm population's temperature.

Figure 9 shows the results of our fitting analysis for all measurements on 15 August 2015 in the same format as Figure 8. The density of the warm population (Figure 9a, red data) is variable and ranges from 10 to 100 cm^{-3}, while the density of the hot population (Figure 9a, blue data) ranges between 0.1 and 1 cm^{-3}. The velocity of the warm population (Figure 9b) ranges from 500 to 1000 km s^{-1}. The temperature of the warm population (Figure 9c, red data) varies between 5×10^4 and 1×10^5 K (4.3–8.6 eV), while the temperature of the hot population (Figure 9c, blue data) varies between 2×10^5 and 1×10^6 K (17.2–86.2 eV). The κ_0 values of the warm population (Figure 9d, red data) vary between 1 and 1000, while most of the hot population κ_0 values (Figure 9d, blue data) vary between 0.1 and 10. Careful inspection of the electron distributions and the fit results suggests that the warm population κ_0 values below 10 are likely unrealistic and the result of the warm distribution attempting to fit the hot population's high-energy tail. The reduced χ^2 of the measurements maintained a baseline of 20 over the entire day, with occasional spikes up to 140.

Table 1. A Summary of the Fitting Results From Measurements on 30 October 2014 and 15 August 2015

d_{Sun}	3 AU		1.3 AU	
d_{Comet}	~20 km		~300 km	
Population	f_W	f_h	f_W	f_h
n (cm^{-3})	10–30	0.005–0.1	10–100	0.1–1
v (km s^{-1})	200–600	N/A	400–800	N/A
T (K)	$1–3\times10^5$	$5–12\times10^5$	$5–10\times10^4$	$2–10\times10^5$
κ_0	10–>1000	0.1–10	10–>1000	0.1–10

Table 1 summarizes the parameters discussed in Figures 8 and 9 and contrasts the physical differences in the electrons around a comet near 3 AU and 1.3 AU. The largest difference is the density of the hot population, which is a factor of 10 larger at 1.3 AU. In contrast, there is only a threefold increase in the warm electron density. The temperature of the warm population is reduced by 50% by the time the comet has reached perihelion. The temperature of the hot population also appears reduced at perihelion, but this may be the result of poor temperature estimation in the fit at 3 AU where the uncertainty is noticeably larger.

4. Discussion

In this study, we have evaluated the suprathermal electron environment near comet 67P/Churyumov-Gerasimenko. Specifically, we used observations from 30 October 2014 when the spacecraft was 20 km from the comet and 3 AU from the Sun, and from 15 August 2015 when the spacecraft was 300 km from the comet and 1.3 AU from the Sun. We then fit observed electron velocity space density with the combination of two three-dimensional kappa distributions and a constant background [*Livadiotis and McComas*, 2009, 2013a, 2013b]. Finally, we characterized the electron environment around the comet, for 2 days near and far from the Sun, with the canonical variables of statistical mechanics.

Our analysis of the suprathermal electron environment around 67P results in the following. 1) The geometric factor of IES' electron sensor has been recalibrated using observations made in flight and expected electron behavior based on previous observations. 2) The electron DEF around 67P was higher at energies below 100 eV far from the Sun and showed more variation over time. 3) The electron environment around 67P is well characterized by the combination of a dense, warm kappa distribution and a rarefied, hot kappa distribution. 4) Far from the Sun, increased heating of the warm population occurred multiple times a day and was often sufficient to obscure the hot electrons. 5) The warm population's density, temperature, and κ_0 values, respectively, increased by a factor 3, decreased by a factor of 2, and remained invariant as the comet approached perihelion. 6) The hot population's density increased by a factor of 10 between observations at 3 AU and 1.3 AU, while the temperature and k_0 values appear invariant with distance.

We have developed a new version of the IES geometric factor that is dependent on the azimuth, elevation, and energy of each individual voxel. There is significant variation in these values, but they typically remain within a factor of 10 of the initial value described by *Burch et al*. [2007]. This is further supported by the densities returned by our fitting analysis, which agree with values measured by *Bame et al*. [1986] and *Zwickl et al*. [1986]. While this calibration enables us to present much improved fits for the energy distribution of the electrons, it should be noted that field-of-view limitations as well as remaining asymmetries limit our ability to derive an unambiguous flow velocity vector, and the values presented should be seen only as upper limits. The new version of the IES' geometric factor is a three-dimensional, $16 \times 16 \times 128$ array, and consequently is too large to share within this document. However, the final version will be made available as soon as possible with the release of IES' level 3 (i.e., differential energy flux) data product on the European Space Agency's Planetary Science Archive. The raw counts returned by IES are already stored in the Planetary Science Archive.

We note that the DEF of electrons above 100 eV was larger when 67P was near 3 AU. *Clark et al*. [2015] found the intensity of electron DEF at lower energies continued to increase until early October and then remained at a high level to the end of their study in early January 2015. Additionally, this result strongly supports the work of *Bodewits et al*. [2015], which finds the inactive coma unexpectedly bright in emission lines OH, OI, CN, NH, and NH_2 and attributes the brightness to dissociative electron impact excitation. This hypothesis might be explored further by comparing the observed brightness in the coma at neighboring time intervals when the observed DEF of electrons was particularly high and low.

The suprathermal electron environment around 67P is well characterized by kappa distributions. In particular, we find very good qualitative agreement between the observed and modeled DEF shown in Figure 7. However, the reduced χ^2 returned by the fitting analysis is rarely below 20 and periodically moves above 100 when the DEF above 100 eV increases. Reduced χ^2 values above 1 suggest that the model is underfitting the observations. It is likely that some of the underfitting is caused by imperfect calibration of the geometric factor discussed in section 2.2. It is also likely that some of the underfitting is caused by real complexity in the observations, because the reduced χ^2 of the fit is well correlated with the temperature of the warm distribution. We speculate that heating of the warm electron population is not isotropic, which is unaccounted for in

our scalar temperature model. One possible explanation for the anisotropic temperature is perpendicular heating caused by the compression and draping of interplanetary magnetic field around the comet. This effect was speculated to have occurred at comet 1P/Halley by *Larson et al*. [1992], who observed that electron flux below 100 eV was enhanced in the perpendicular direction. Another possibility is that the electrons are heated through wave-particle interactions, which are known to cause anisotropic heating [*Thomsen et al*., 1986; *Shapiro et al*., 1999; *Clark et al*., 2015].

The DEF of electrons near 100 eV periodically increases when the comet was far from the Sun. The periodicity is generally 12 h, but is not always clear, as some flux increases may be associated with solar wind drivers [*Clark et al*., 2015]. The 12 h periodicity suggests that it is associated with similarly periodic neutral density enhancements in the coma observed by the Comet Pressure Sensor (COPS) [*Hässig et al*., 2015]. *Edberg et al*. [2015] found that the electron density, observed by LAP and MIP, increased with the neutral density and showed a similar 6 h periodicity. However, our fitting analysis shows that most of the increase in flux is caused by an increase in the warm population's temperature and not from an increase in density. The IES probably does not observe density increases because the majority of the electrons are below the observed energy range (4.3–18,000 eV). Moreover, we exclude all data below 10 eV from our fitting analysis because of the poorly understood effect of spacecraft charging. This result is in strong agreement with *Zwickl et al*. [1986], who found three electron populations; the coldest of which had a temperature of only a few eV and would likely have been unobservable by IES. It is unclear if the cold population observed by *Zwickl et al*. is the same as the population observed by LAP on Rosetta, but it seems likely.

The strong correlation found between electron densities observed by LAP and MIP and neutral densities observed by COPS suggests that the bulk of the cold population is cometary photoelectrons. Model predictions indicate that cometary photoelectrons should produce a convolution of shell distributions between 20 and 30 eV and a thermalized distribution observable by IES [*Gan and Cravens*, 1990; *Burch et al*., 2007]. The discrepancy between our observations and model predictions presents an unexpected open question. What is the source of the warm electrons observed in this work and by *Zwickl et al*. [1986]? We hypothesize two possible explanations. 1) Warm electrons are also the cometary photoelectrons but transitioning from their nascent velocity distribution into a colder, thermally equilibrated state that IES does not observe. A transitional state approaching thermal equilibrium is supported by the calculated κ_0 values of the warm population (i.e., 10–>1000), which suggests that they are slightly out of thermal equilibrium and consequently experiencing heating or cooling. This was further studied by *Madanian et al*. [2016], which used ambipolar electric field and plasma compression to explain the buildup of cold electron population near the comet 67P. 2) Warm electrons are locally heated from the unobserved reservoir of cold electrons, perhaps through wave-particle interactions as suggested by *Thomsen et al*. [1986] and *Clark et al*. [2015]. *Richter et al*. [2015] and *Volwerk et al*. [2016] have observed waves at 67P, but these waves are likely too low in frequency to significantly affect the electrons.

The density of the warm electron population increased by a factor of 3 as the comet approached the Sun. The comet was more active at perihelion, but the spacecraft was also a factor of 10 farther from the comet than in October 2014. Comparing the COPS neutral density between 30 October 2014 and 15 August 2015, we find that the local neutral densities are ~10^7 cm^{-3} on both days. We speculate that the increase in warm electron population density relative to the neutral density may be explained by the increased photoionization rate of the comet closer to the Sun. Solar irradiance is proportional to r^{-2}, which increases the light intensity by a factor of 5.3 from 3 AU to 1.3 AU. In contrast, the temperature of the warm population cooled by a factor of 2 as 67P approached perihelion. The warm population temperature on 30 October 2014 and 15 August 2015, respectively, matches those found by *Zwickl et al*. [1986] in the midpopulation far from the comet and at closest approach. The ICE mission traveled through the coma of G-Z over a few hours. In contrast, Rosetta has remained in a relatively fixed location, while 67P's coma expanded around it. The κ_0 values for the warm population are invariant with heliocentric distance, and in the range of 10–>1000. For the warm population, the values of κ_0 suggest that the warm population is near thermal equilibrium, but some heating or cooling is occurring. It is also interesting to note how quickly the values change. The values can change from 10 to 1000 in a single measurement cycle, suggesting that this state is dynamic.

The hot population density increases by a factor 10 between 3 AU and 1.3 AU. Additionally, the temperature of the hot population appears invariant with heliocentric distance. The κ_0 values of the hot population are

stable and consistently in the range of 1–10 on both days included in this study. Our observations of the hot population density, temperature, and κ_0 values closely agree with observations of solar wind halo electrons between 1 and 3 AU [*McComas et al*., 1992; *Štverák et al*., 2009]. Consequently, our result supports the conclusion of *Zwickl et al*. [1986]; the hot electron population originates in the solar wind.

5. Conclusions

We presented the first characterization of cometary electrons using statistical mechanics for systems out of thermal equilibrium. We found that there are at least three populations of electrons near 67P, and only two of which are observable by IES. Both observable populations are well characterized by kappa distributions, which we define as a dense, warm population and a rarefied, hot population. However, it seems likely that some anisotropic heating is occurring, which we intend to study in future work by fitting the observations with bikappa distributions. The rarefied, hot population is very likely to be solar wind halo electrons impinging upon the coma along draped interplanetary magnetic field lines. The dense, warm population is much less well understood. We speculate that the warm population might be cometary photoelectrons transitioning from their early state into a more stable distribution, or that they might be heated from the unobserved, cold population.

Acknowledgments
Rosetta is a European Space Agency (ESA) mission with support by member nations and U.S. National Aeronautics and Space Administration (NASA). The work on IES was supported, in part, by NASA through contract 1345493 with the Jet Propulsion Laboratory, California Institute of Technology. We thank the teams at Imperial College London and ESA who have been responsible for the operation of IES. All of the data shown from the Rosetta mission can be found on the European Space Agency's Planetary Science Archive (http://www.rssd.esa.int/index.php?project=PSA&page=ftpaccess) with the exception of the kappa function fit parameters to the electron distributions, which can be requested from the author at tbroiles@swri.edu.

References

Acton, C. H. (1996), Ancillary data services of NASA's navigation and ancillary information facility, *Planet. Space Sci.*, *44*(1), 65–70, doi:10.1016/0032-0633(95)00107-7.

Ashihara, O. (1978), Photoelectron fluxes in cometary atmospheres, *Icarus*, *35*(3), 369–384, doi:10.1016/0019-1035(78)90089-1.

Bame, S. J., et al. (1986), Comet Giacobini-Zinner: Plasma description, *Science*, *232*(4748), 356–361, doi:10.1126/science.232.4748.356.

Behar, E., H. Nilsson, G. S. Wieser, Z. Nemeth, T. W. Broiles, and I. Richter (2016), Mass loading at 67P/Churyumov-Gerasimenko: A case study, *Geophys. Res. Lett.*, 1411–1418, doi:10.1002/2015GL067436.

Bodewits, D., L. M. Lara, F. LaForgia, M. F. A'Hearn, J. Knollenberg, M. Lazzarin, Z.-Y. Lin, and X. Shi (2015), Observed changes in the physical environment and chemistry in the inner coma of 67P/Churyumov-Gerasimenko, Paper presented at the Division of Planetary Sciences, Washington, D.C., vol. 47, p. 503.03. [Available at http://adsabs.harvard.edu/abs/2015DPS....4750303B.]

Broiles, T. W., J. L. Burch, G. Clark, C. Koenders, E. Behar, R. Goldstein, S. A. Fuselier, K. E. Mandt, P. Mokashi, and M. Samara (2015), Rosetta observations of solar wind interaction with the comet 67P/Churyumov-Gerasimenko, *Astron. Astrophys.*, *583*, 7, doi:10.1051/0004-6361/201526046.

Burch, J. L., R. Goldstein, T. E. Cravens, W. C. Gibson, R. N. Lundin, C. J. Pollock, J. D. Winningham, and D. T. Young (2007), RPC-IES: The ion and electron sensor of the Rosetta plasma consortium, *Space Sci. Rev.*, *128*(1-4), 697–712, doi:10.1007/s11214-006-9002-4.

Burch, J. L., T. E. Cravens, K. Llera, R. Goldstein, P. Mokashi, C.-Y. Tzou, and T. Broiles (2015), Charge exchange in cometary coma: Discovery of H- ions in the solar wind close to comet 67P/Churyumov-Gerasimenko, *Geophys. Res. Lett.*, *42*, 5125–5131, doi:10.1002/2015GL064504.

Clark, G., et al. (2015), Suprathermal electron environment of comet 67P/Churyumov-Gerasimenko: Observations from the Rosetta ion and electron sensor, *Astron. Astrophys.*, *583*, 6, doi:10.1051/0004-6361/201526351.

Cravens, T. E. (1987), Theory and observations of cometary ionospheres, *Adv. Space Res.*, *7*, 147–158, doi:10.1016/0273-1177(87)90212-2.

Cravens, T. E. (1991), Collisional processes in cometary plasmas, in *Cometary Plasma Processes*, edited by A. Johnstone, pp. 27–35, AGU, Washington, D. C.

Cravens, T. E., J. U. Kozyra, A. F. Nagy, T. I. Gombosi, and M. Kurtz (1987), Electron impact ionization in the vicinity of comets, *J. Geophys. Res.*, *92*(7), 7341–7353, doi:10.1029/JA092iA07p07341.

Edberg, N. J. T., et al. (2015), Spatial distribution of low-energy plasma around comet 67P/CG from Rosetta measurements, *Geophys. Res. Lett.*, *42*, 4263–4269, doi:10.1002/2015GL064233.

Eriksson, A. I., et al. (2006), RPC-LAP: The Rosetta Langmuir probe instrument, *Space Sci. Rev.*, *128*(1-4), 729–744, doi:10.1007/s11214-006-9003-3.

Feldman, W. C. (1985), Electron velocity distributions near collisionless shocks, in *Collisionless Shocks in the Heliosphere: Reviews of Current Research*, edited by B. T. Tsurutani and R. G. Stone, pp. 195–205, AGU, Washington, D. C.

Feldman, W. C., R. C. Anderson, S. J. Bame, S. P. Gary, J. T. Gosling, D. J. McComas, M. F. Thomsen, G. Paschmann, and M. M. Hoppe (1983), Electron velocity distributions near the Earth's bow shock, *J. Geophys. Res.*, *88*, 96–110, doi:10.1029/JA088iA01p00096.

Gan, L., and T. E. Cravens (1990), Electron energetics in the inner coma of comet Halley, *J. Geophys. Res.*, *95*, 6285–6303, doi:10.1029/JA095iA05p06285.

Goldstein, R., et al. (2015), The Rosetta Ion and Electron Sensor (IES) measurement of the development of pickup ions from comet 67P/Churyumov-Gerasimenko, *Geophys. Res. Lett.*, *42*, 3093–3099, doi:10.1002/2015GL063939.

Häberli, R. M., K. Altwegg, H. Balsiger, and J. Geiss (1996), Heating of the thermal electrons in the coma of comet P/Halley, *J. Geophys. Res.*, *101*(A7), 15,579–15,589, doi:10.1029/96JA01191.

Hässig, M., et al. (2015), Time variability and heterogeneity in the coma of 67P/Churyumov-Gerasimenko, *Science*, *347*(6220, aaa0276), doi:10.1126/science.aaa0276.

Larson, D. E., K. A. Anderson, R. P. Lin, C. W. Carlson, H. Réme, K.-H. Glassmeier, and F. M. Neubauer (1992), Electron distributions upstream of the comet Halley bow shock: Evidence for adiabatic heating, *J. Geophys. Res.*, *97*, 2907–2916, doi:10.1029/91JA02698.

Livadiotis, G. (2015), Kappa distribution in the presence of a potential energy, *J. Geophys. Res. Space Physics*, *120*, 880–903, doi:10.1002/2014JA020671.

Livadiotis, G., and D. J. McComas (2009), Beyond kappa distributions: Exploiting Tsallis statistical mechanics in space plasmas, *J. Geophys. Res.*, *114*, A11105, doi:10.1029/2009JA014352.

Livadiotis, G., and D. J. McComas (2011), Invariant kappa distribution in space plasmas out of equilibrium, *Astrophys. J.*, *741*(2), 88, doi:10.1088/0004-637X/741/2/88.

Livadiotis, G., and D. J. McComas (2013a), Understanding kappa distributions: A toolbox for space science and astrophysics, *Space Sci. Rev.*, *175*(1-4), 183–214, doi:10.1007/s11214-013-9982-9.
Livadiotis, G., and D. McComas (2013b), Evidence of large-scale quantization in space plasmas, *Entropy*, *15*(3), 1118–1134, doi:10.3390/e15031118.
Madanian, H., et al. (2016), Suprathermal electrons near the nucleus of comet 67P/Churyumov-Gerasimenko at 3 AU: Model comparisons with Rosetta data, *J. Geophys. Res. Space Physics*, *121*, 5815–5836, doi:10.1002/2016JA022610.
Maksimovic, M., et al. (2005), Radial evolution of the electron distribution functions in the fast solar wind between 0.3 and 1.5 AU, *J. Geophys. Res.*, *110*, A09104, doi:10.1029/2005JA011119.
Marconi, M. L., and D. A. Mendis (1986), The electron density and temperature in the tail of comet Giacobini-Zinner, *Geophys. Res. Lett.*, *13*(4), 405–406, doi:10.1029/GL013i004p00405.
McComas, D. J., S. J. Bame, W. C. Feldman, J. T. Gosling, and J. L. Phillips (1992), Solar wind halo electrons from 1–4 AU, *Geophys. Res. Lett.*, *19*(12), 1291–1294, doi:10.1029/92GL00631.
Mendis, D. A., and M. Horányi (2013), Dusty plasma effects in comets: Expectations for Rosetta, *Rev. Geophys.*, *51*, 53–75, doi:10.1002/rog.20005.
Nilsson, H., et al. (2015), Birth of a comet magnetosphere: A spring of water ions, *Science*, *347*(6220, aaa0571), doi:10.1126/science.aaa0571.
Odelstad, E., A. I. Eriksson, N. J. T. Edberg, F. Johansson, E. Vigren, M. André, C.-Y. Tzou, C. Carr, and E. Cupido (2015), Evolution of the plasma environment of comet 67P from spacecraft potential measurements by the Rosetta Langmuir probe instrument, *Geophys. Res. Lett.*, *42*, 10,126–10,134, doi:10.1002/2015GL066599.
Richter, I., et al. (2015), Observation of a new type of low frequency waves at Comet 67P/Churyumov-Gerasimenko, *Ann. Geophys.*, *33*(8), 1031–1036, doi:10.5194/angeo-33-1031-2015.
Rubin, M., M. R. Combi, L. K. S. Daldorff, T. I. Gombosi, K. C. Hansen, Y. Shou, V. M. Tenishev, G. Tóth, B. van der Holst, and K. Altwegg (2014), Comet 1P/Halley multifluid MHD model for the Giotto fly-by, *Astrophys. J.*, *781*(2), 86, doi:10.1088/0004-637X/781/2/86.
Scudder, J. D. (1995), A review of the physics of electron heating at collisionless shocks, *Adv. Space Res.*, *15*(8–9), 181–223, doi:10.1016/0273-1177(94)00101-6.
Shapiro, V. D., R. Bingham, J. M. Dawson, Z. Dobe, B. J. Kellett, and D. A. Mendis (1999), Energetic electrons produced by lower hybrid waves in the cometary environment and soft X ray emission: Bremsstrahlung and K shell radiation, *J. Geophys. Res.*, *104*(A2), 2537–2554, doi:10.1029/1998JA900047.
Štverák, Š., M. Maksimovic, P. M. Trávníček, E. Marsch, A. N. Fazakerley, and E. E. Scime (2009), Radial evolution of nonthermal electron populations in the low-latitude solar wind: Helios, Cluster, and Ulysses observations, *J. Geophys. Res.*, *114*, A05104, doi:10.1029/2008JA013883.
Thomsen, M. F., S. J. Bame, W. C. Feldman, J. T. Gosling, D. J. McComas, and D. T. Young (1986), The comet/solar wind transition region at Giacobini-Zinner, *Geophys. Res. Lett.*, *13*(4), 393–396, doi:10.1029/GL013i004p00393.
Trotignon, J. G., et al. (2006), RPC-MIP: The mutual impedance probe of the Rosetta plasma consortium, *Space Sci. Rev.*, *128*(1-4), 713–728, doi:10.1007/s11214-006-9005-1.
Tsallis, C. (1988), Possible generalization of Boltzmann-Gibbs statistics, *J. Stat. Phys.*, *52*(1-2), 479–487, doi:10.1007/BF01016429.
Vasyliunas, V. M. (1968), A survey of low-energy electrons in the evening sector of the magnetosphere with OGO 1 and OGO 3, *J. Geophys. Res.*, *73*(9), 2839–2884, doi:10.1029/JA073i009p02839.
Vigren, E., and M. Galand (2013), Predictions of ion production rates and ion number densities within the diamagnetic cavity of Comet 67P/Churyumov-Gerasimenko at perihelion, *Astrophys. J.*, *772*(1), 33, doi:10.1088/0004-637X/772/1/33.
Volwerk, M., et al. (2016), Mass-loading, pile-up, and mirror-mode waves at comet 67P/Churyumov-Gerasimenko, *Ann. Geophys.*, *34*(1), 1–15, doi:10.5194/angeo-34-1-2016.
Zwickl, R. D., D. N. Baker, S. J. Bame, W. C. Feldman, S. A. Fuselier, W. F. Huebner, D. J. McComas, and D. T. Young (1986), Three component plasma electron distribution in the intermediate ionized coma of comet Giacobini-Zinner, *Geophys. Res. Lett.*, *13*(4), 401–404, doi:10.1029/GL013i004p00401.

Erratum

In the originally published version of this article, equations (5) and (6) were incorrect. They have since been corrected, and this version may be considered the authoritative version of record.